analytical chemistry

Article

Cite This: Anal. Chem. XXXX, XXX, XXX−XXX

pubs.acs.org/ac

Acid-Promoted D-A-D Type Far-Red Fluorescent Probe with High Photostability for Lysosomal Nitric Oxide Imaging

Fengyang Wang,[†,‡] Shujuan Yu,[†,§] Zhiai Xu,[*,‡] Lingling Li,[‡] Yijing Dang,[‡] Xiaowei Xu,[∥] Yi Luo,[∥] Zhen Cheng,[⊥] Haijun Yu,[#] Wen Zhang,[‡] Ao Zhang,[§,#] and Chunyong Ding[*,§,#]

[‡]School of Chemistry and Molecular Engineering, East China Normal University, Shanghai 200241, China

[§]CAS Key Laboratory of Receptor Research, Synthetic Organic and Medicinal Chemistry Laboratory, Shanghai Institute of Materia Medica, Chinese Academy of Sciences, Shanghai 201203, China

[∥]State Key Laboratory of Fine Chemicals, School of Chemical Engineering, Dalian University of Technology, Dalian 116024, China

[⊥]Molecular Imaging Program at Stanford (MIPS), Bio-X Program, and Department of Radiology, Stanford University, Stanford, California 94305-5344, United States

[#]State Key Laboratory of Drug Research, Shanghai Institute of Materia Medica (SIMM), Chinese Academy of Sciences, Shanghai 201203, China

Supporting Information

ABSTRACT: To accurately monitor the variations of lysosomal nitric oxide (NO) under physiological condition remains a great challenge for understanding the biological function of NO. Herein, we developed a new chemotype probe, namely, MBTD, for acid-promoted and far-red fluorescence imaging of lysosomal NO in vitro and ex vivo. MBTD was rationally designed by incorporating *o*-phenylenediamino (OPD) moiety into the donor−acceptor−donor (D-A-D) type fluorophore based on a dual intramolecular charge transfer (ICT) mechanism. Compared to previously reported OPD-based NO probes, MBTD displays several distinct advantages including large stroke shift, huge on−off ratio with minimal autofluorescence, and high NO specificity. Particularly, MBTD exhibits an acid-promoted response to NO with high acid tolerance, which greatly improves the spatial resolution to lysosomal NO by excluding the background noise from other nonacidic organelles. Furthermore, MBTD displayed much longer-lived and more stable fluorescence emission in comparison with the commercialized NO probe. MBTD was employed for ratiometric examination of the exogenous or endogenous NO of macrophages. More importantly, MBTD was able to detect the variation of lysosomal NO level in an acute liver injury mouse model ex vivo, implying the potential of MBTD for real-time monitoring the therapeutic efficacy of drug candidates for the treatment of acute liver injury. MBTD as a novel type of NO probe might open a new avenue for precisely sensing lysosomal NO-related pathological and therapeutic process.

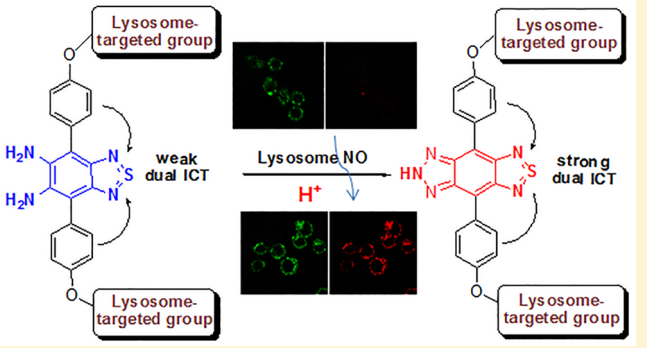

Nitric oxide (NO) as a critical signaling molecular participates in a large variety of physiological processes including inflammation, blood pressure regulation, neurotransmission, and immunomodulation.[1−7] The impairment of intracellular NO homeostasis can induce a variety of pathological conditions. Accumulating evidence indicates the biological effects of NO are closely associated with its concentration and diffusion dynamics in the subcellular organelles (e.g., mitochondria and lysosome).[8−12] It was reported that lysosomal functions such as catabolic autophagy process are affected by NO.[11] To fully elucidate the physiological roles of lysosomal NO, it is highly desirable but challenging to develop an accurate method for in situ detection of NO in complicated biological condition, particularly in tissues and living organisms, due to the highly diffusible and reactive characteristics of NO, as well as the acidic microenvironment of lysosomal vesicles.

Of the reported techniques for detection of highly reactive species,[13−35] the fluorimetric strategy has attracted extensive attention due to its high selectivity and sensitivity, as well as real-time and noninvasive visualization of biological NO.[13−33] Accordingly, a range of fluorescent NO probes have been developed by coupling a NO-capturing moiety to organic fluorophores such as rhodamine,[23−28] naphthalimide,[29] and BODIPY derivatives.[30−32] The *o*-phenylenediamino (OPD) moiety is the most commonly used NO-capturing moiety, which not only serves as a fluorescence quencher through

Received: February 5, 2018
Accepted: May 31, 2018

DOI: 10.1021/acs.analchem.8b00612
Anal. Chem. XXXX, XXX, XXX−XXX

photoinduced electron transfer (PET), but also specifically reacts with NO under aerobic conditions to form benzotriazoles, thus, restoring the fluorescence signals of fluorophore by inhibiting the PET process.[36] Despite being promising, the application of the OPD-based probes for imaging lysosomal NO were hindered by their intrinsic drawbacks such as intolerance of the acidic pH, susceptibility to other reactive species, low organelle specificity and poor photostability. Moreover, most of these PET probes suffered from the short emission wavelength (<600 nm), which restricts the in situ tracking of NO in deep tissue and living organisms with strong background autofluorescence. As such, various fluorescence NO probes with improved sensing performance have been developed recently.[37−46] Nevertheless, few of them could be utilized for accurately quantifying the variation of lysosomal NO levels due to the interference of photobleaching, subcellular microenvironment, and local probe concentration variation.

The development of ratiometric fluorescent probe is a practical solution to address the above concerns. Ratiometric fluorescent imaging can synchronously record two signals at different wavelengths, thus, providing a built-in reference to get rid of the interference. Until now, ratiometric NO probes with long wavelength emission (>600 nm) have barely been reported.[23,47] To this end, we herein present a novel OPD-based fluorescent NO probe with far-red emission, namely, MBTD (4,7-bis(4-(2-morpholinoethoxy)phenyl)benzo[*c*]-[1,2,5] thiadiazole-5,6-diamine), for ratiometirc examination of lysosomal NO in vitro and ex vivo. MBTD is designed based on a dual intramolecular charge transfer (ICT) mechanism by integrating the OPD moiety into a donor−acceptor−donor (D-A-D) type fluorophore as the weak electron acceptor. To our knowledge, D-A-D type fluorescent probes with far-red emission have not been reported for in situ monitoring lysosomal NO. MBTD not only possesses high acid-tolerance and acid-promoted response to NO for fluorescent NO imaging specifically in lysosomes, but also shows the intrinsic potential for detecting NO of deep tissue. Moreover, MBTD exhibits excellent photostability and high NO selectivity arising from the unique D-A-D structure, suggesting a good potential of MBTD as a new chemotype of fluorescent probe for accurate sensing of lysosomal NO.

EXPERIMENTAL SECTION

Preparation of Reactive Oxygen/Nitrogen Species. NO solution was prepared by bubbling NO gas to deoxygenated water. The concentration of NO saturated solution was measured by Griess Method. Nitrite (NO_2^-) and nitrate (NO_3^-) were prepared by dissolving sodium nitrite and sodium nitrate in deionized water. Hydroxyl radical ($^{\bullet}OH$) was generated by Fenton reaction (Fe^{2+}/H_2O_2 = 1:6 mM). Hypochloride anion (ClO^-) was prepared by NaClO. O_2^- was generated from KO_2 solid diluted in DMSO. TBHP (*tert*-butyl hydroperoxide) solution was prepared by diluting TBHP. H_2O_2 solution (1 mM) was provided by diluting 30% H_2O_2. Peroxynitrite ($ONOO^-$) solution was generated by H_2O_2 solution (1 mM) reacting with $NaNO_2$ (1 mM). The single oxygen ($^1O_2$) was produced by reaction between NaClO (1 mM) and H_2O_2 (1 mM).

Cell Culture and Cytotoxicity Assay. RAW 264.7 cells were obtained from cell bank of Chinese Academy of Sciences (Shanghai, China). RAW 264.7 cells were cultured in DMEM medium with 1% penicinllin/streptomycin and 10% fetal bovine serum (FBS) in an atmosphere of 5% CO_2 at 37 °C. The cell cytotoxicity of MBTD was evaluated by MTT assay. One $\times 10^4$ cells per well were seeded on 96-well plates and incubated for 24 h at 37 °C under 5% CO_2. MBTD at concentrations of 0−15 μM was added to the wells and incubated for 24 h. After that, the supernatant was removed and cells were washed three times with 10 mM PBS buffer. Subsequently, 0.5 mg/mL MTT was added and incubated for additional 4 h. Finally, the formazan crystal was dissolved by DMSO and the absorbance values were recorded at 570 nm using a plate reader.

Fluorescence Imaging. For fluorescence imaging in vitro, cells were seeded on 35 mm glass-bottom culture dishes with 8000 cells per well and incubated for 24 h at 37 °C. The cells were treated with 5 μM MBTD for 1 h. After washing three times with 10 mM PBS buffer, the cells were incubated with various concentration of DEANO (NO donor) for 1 h. Finally, the cells were washed four times with PBS buffer and observed with confocal laser scanning microscopic (CLSM). For imaging of endogenous NO in RAW 264.7 cells, the cells were preincubated with 10 μg/mL LPS for 5 h, then stained with 5 μM MBTD for 1 h. To confirm the production of NO, the cells were also treated with 10 μg/mL hemoglobin for 2 h for comparison. After that, the cells were washed with PBS buffer and imaged. In order to confirm the lysosome-targeting ability of probe MBTD, cells were stained with 5 μM probe MBTD for 1 h and incubated with 400 nM LysoTracker Red, 50 nM MitoTracker Red separately for 1 h. The cells were also incubated with 1 μM Baf-A1 for 2 h and incubated with 5 μM MBTD for 1 h. For photostability study of different probes, the cells were incubated with 5 μM probe MBTD or DAF-FM-DA, and then treated with 100 μM DEANO for 1 h, finally the fluorescence images were recorded. The mean fluorescence intensity was analyzed with ImageJ Software.

Acute Liver Injury and Imaging of Frozen Tissue Slices Ex Vivo. Male Balb/c mice (6−8 week old, 18−20 g) were obtained from Animal Center of Shanghai Institute of Material Medica, Chinese Academy of Sciences. All animal procedures were carried out under the guidelines approved by the Institutional Animal Care and Use Committee (IACUC) of the Shanghai Institute of Material Medica, Chinese Academy of Sciences. The mice were not given food and water for 12 h to avoid the possible interferences of food. A total of 12 mice were randomly divided into four groups. Control group includes three mice. Test group includes nine mice. (a) Control group: The mice were injected intraperitoneally with 200 μL of 0.9% NaCl for 6 h. (b) LPS group: The mice were injected with 0.9% NaCl containing 5 μg/kg LPS and 300 mg/kg D-GalN for 6 h. (c) LPS+NAC group: The mice were injected with 5 μg/kg LPS and 300 mg/kg D-GalN for 2 h, then with 300 mg/kg NAC for 4 h. (d) L-NAME+LPS group: The mice were injected with 50 μg/mL L-NAME for 6 h and then injected 5 μg/kg LPS and D-GalN for 6 h. After that, the mice were killed using 10 mg/mL sodium pentobarital and the liver tissues were embedded in OCT. Then the tissues were cut into 4-μm-thick slices at −30 °C. The tissue slices were stained with 10 μM MBTD for 1 h and incubated with 5 μg/mL DAPI for 5 min. Finally, the treated tissue slices were observed with CLSM.

RESULTS AND DISCUSSION

Design and Synthesis of the D-A-D Type NO Probe. The D-A-D architecture employed for fluorescent probe design is featured with a series of distinct optical properties including

DOI: 10.1021/acs.analchem.8b00612
Anal. Chem. XXXX, XXX, XXX−XXX

Scheme 1. Strategies of the OPD-Based Fluorescent Probe for NO Based on Different Mechanisms: (A) Previous Probes Based on PET; (B) D-A-D Type Probe MBTD of This Work Based on ICT

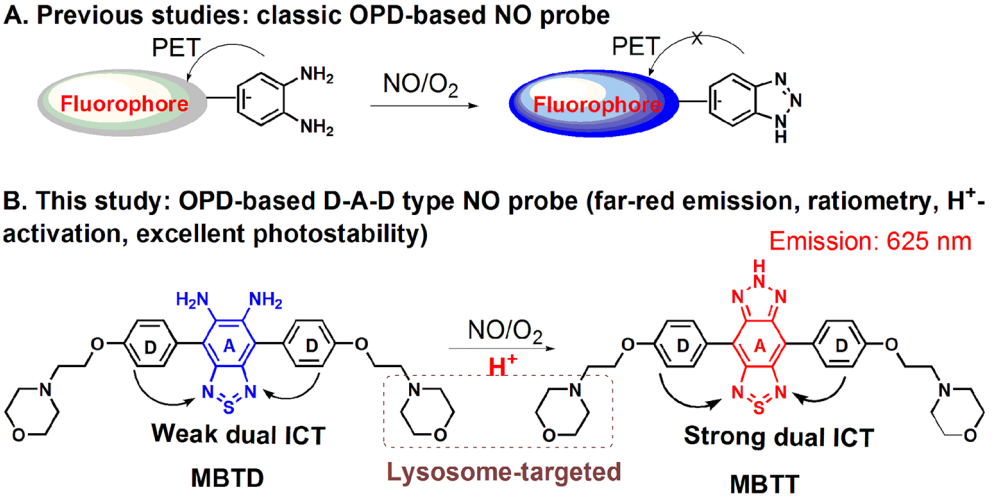

Scheme 2. Synthesis of Compounds MOBTD, MBTD, and MBTT[a]

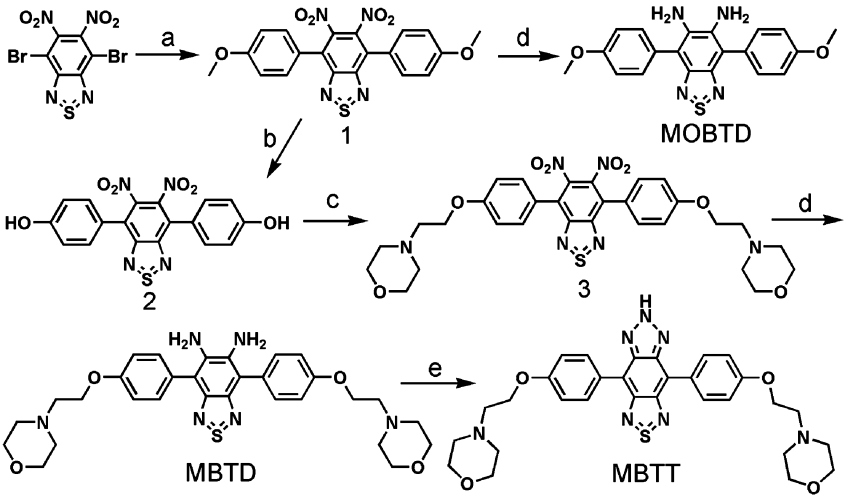

[a]Conditions and reagents: (a) (4-methoxyphenyl)boronic acid, $Pd(PPh_3)_4$, K_2CO_3, toluene, 110 °C; (b) BBr_3, DCM, −78 °C; (c) 4-(2-bromoethyl)morpholine, NaH, DMF; (d) Fe/ACOH; (e) $NaNO_2$/HOAc.

significant absorption and emission in the red or near-infrared (NIR) region, large Stokes' shift, and high photostability.[48−50] The benzo(1,2-*c*:4,5-*c*′)bis([1,2,5]thiadiazole) core has commonly been used as the electron acceptor of D-A-D compound due to its substantial quinoid character and great electron delocalization.[51−54] Inspired by this, we employed thiadiazole-fused OPD (TOPD) scaffold as both the NO-capturing moiety and the weak electron acceptor for MBTD design. Moreover, two alkyoxyl groups severing as the electron donors were linked to the 4- and 8-positions of TOPD via a benzene unit as a π spacer, and followed by two morpholinyl groups for specifically targeting lysosomes (Scheme 1). It is envisioned that, upon reaction with NO, TOPD is transferred into the tricyclic thiadiazole-fused benzotriazole as another electron acceptor with stronger electron-withdrawing ability,[49] and the resulting product MBTT possesses an enhanced ICT ability, leading to a large red-shift of the excition/emission wavelengths.

The MBTD probe was synthesized by Suzuki coupling of 4,7-dibromo-5,6-dinitrobenzo[*c*][1,2,5]thiadiazole with (4-methoxyphenyl)boronic acid (Scheme 2). Demethylation of **1** with BBr_3 followed by nucleophilic substitution reaction with 4-(2-bromoethyl)morpholine provided the precursor **3**, which then underwent Fe/AcOH-mediated reduction reaction to furnish MBTD. Further reaction of MBTD with $NaNO_2$/HOAc gave rise to the fluorescent product MBTT. To determine if the morpholinyl groups account for the lysosome-targeting ability of MBTD, another probe MOBTD was synthesized as a comparison according to the similar procedure. All synthesized final compounds were characterized by ^{1}H NMR, ^{13}C NMR spectroscopy, and LR/HR-ESI-MS, respectively (Figures S1, S2, S4, and S5). HPLC chromatogram showed MBTD has a high purity of 96.9% (Figure S3).

Photophysical Properties of MBTD. The photophysical properties of MBTD were first investigated by using UV−vis and fluorescence spectroscopic examinations, respectively. MBTD showed UV−vis absorbance peaked at 365 nm and moderate fluorescence emission at 565 nm (λ_{ex} = 365 nm) due to the weak ICT process induced by TOPD (Figures 1A and S9A). Negligible fluorescence emission was detected in aqueous solution of MBTD when excited at 488 nm (Figure 1B),

DOI: 10.1021/acs.analchem.8b00612
Anal. Chem. XXXX, XXX, XXX−XXX

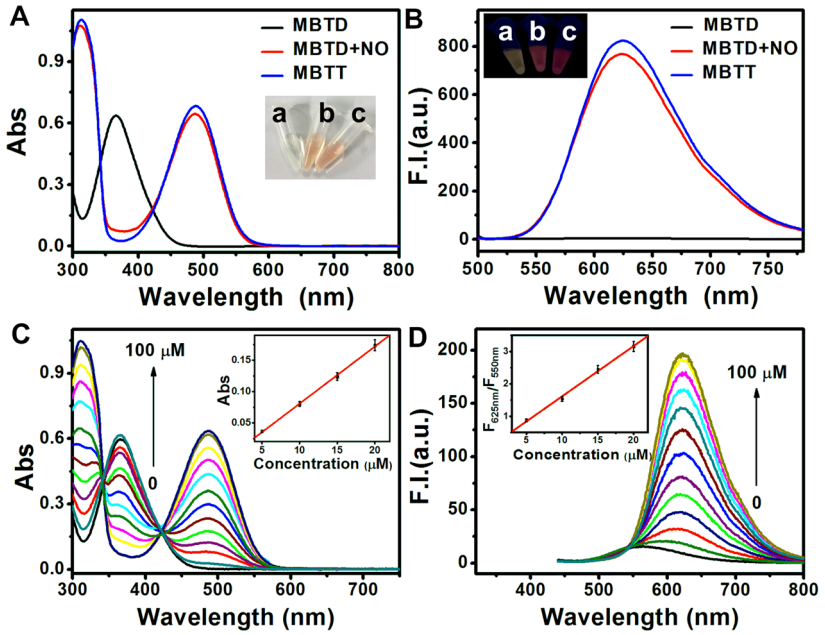

Figure 1. (A) UV−vis absorbance and (B) fluorescence spectra of 50 μM MBTT and MBTD in the absence and presence of NO (100 μM) under the aerobic condition, λ_{ex} = 488 nm. Inset: the photographs of MBTD probe (a), MBTD in the presence of NO (b), and the product MBTT (c). (C) Absorbance spectra of MBTD probe (50 μM) upon the addition of different concentrations of NO. (D) Fluorescence response of probe MBTD in the presence of various concentration of NO, λ_{ex} = 421 nm. Inset: Plot of F_{625nm}/F_{550nm} ratio of NO-incubated MBTD against NO concentration (5−20 μM). Buffer: 10 mM PB (pH = 5.0, 10% DMAC).

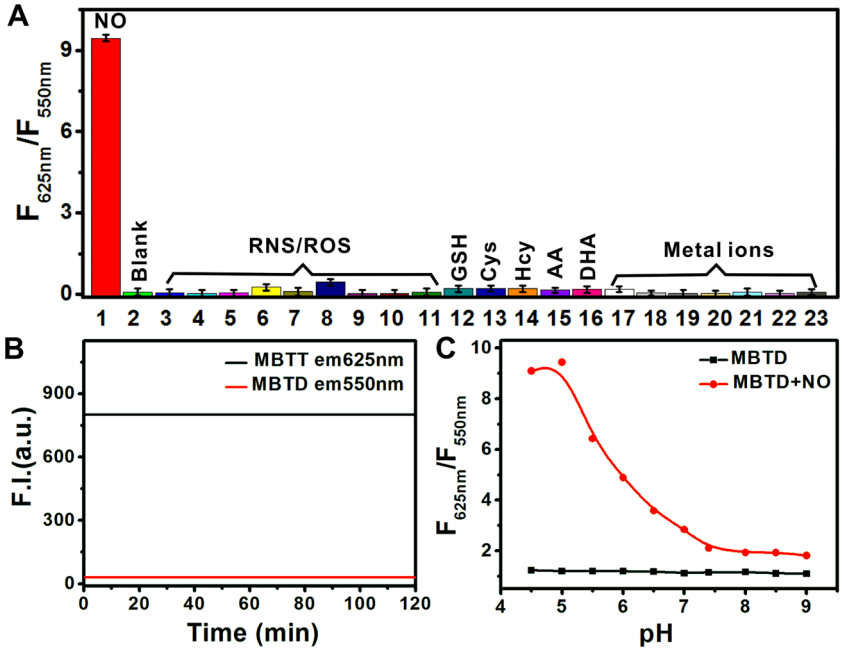

Figure 2. (A) Fluorescence responses (F_{625nm}/F_{550nm}) of MBTD (50 μM) incubated with 100 μM NO, 1 mM ROS/RNS 2−11 (blank, NO_2^-, NO_3^-, $^{\bullet}OH$, ClO^-, TBHP, H_2O_2, $O_2^{\bullet-}$, $^1O_2$, $ONOO^-$), 1 mM active biomolecules 12−16 (GSH, Cys, Hcy, AA, DHA), and 1 mM metal ions 17−23 (K^+, Na^+, Ca^{2+}, Fe^{2+}, Fe^{3+}, Zn^{2+}, Mg^{2+}). Reaction time: 30 min, λ_{ex} = 421 nm. (B) Photostability of 50 μM MBTD (λ_{ex} = 365 nm, red line) and 50 μM MBTT (λ_{ex} = 488 nm, black line). Buffer: 10 mM PB (pH = 5.0, 10% DMAC). (C) Effects of pH on F_{625nm}/F_{550nm} ratio of MBTD in the absence or presence of 100 μM NO, λ_{ex} = 421 nm.

verifying minimal basal level autofluorescence of MBTD. In contrast, upon addition of 100 μM NO under aerobic condition, the maximum absorption was considerably red-shifted to 488 nm together with obvious color change from yellow-green to red under the ultraviolet lamp (Figure 1A,B). The corresponding fluorescence emission peak dramatically shifted to 625 nm (λ_{ex} = 488 nm) with a 446-fold off−on ratio (Figure 1B), which could be attributed to an enhanced ICT process by the resulting thiadiazole-fused benzotriazole as stronger electron acceptor. The effect of O_2 on the fluorescence responses was investigated. As shown in Figure S6, the absorbance and fluorescence responses are significantly suppressed at low concentration of O_2 by bubbling pure N_2 gas. In the case of bubbling pure O_2 gas, the response decreases

DOI: 10.1021/acs.analchem.8b00612
Anal. Chem. XXXX, XXX, XXX−XXX

Scheme 3. Proposed Mechanism for Acid-Promoted Fluorescence Property of MBTT

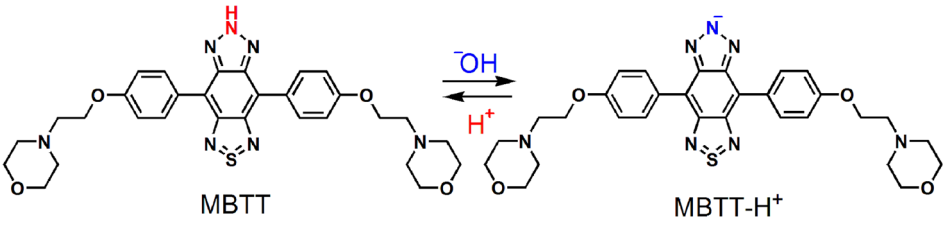

Table 1. Structures and Energies of the HOMO and LUMO of MBTD, MBTT, and MBTT-H$^+$ at the B3LYP/6-31+G (d) Level in the Gas Phase[a]

Compound	HOMO	Energy (eV)	LUMO	Energy (eV)	E_{gap} (eV)
MBTD		-5.15		-1.66	3.48
MBTT		-4.91		-2.77	2.14
MBTT–H$^+$		-1.99		0.30	2.29

[a] $E_{gap} = E_{LUMO} - E_{HOMO}$.

slightly, and this was probably ascribed to oxidization of minor NO into NO_2. These results demonstrated that O_2 is crucial for the reaction. To validate the reaction mechanism we proposed, MBTT was synthesized by reaction of MBTD with $NaNO_2$ in glacial acetic acid (Scheme 2), and we found its absorption and emission maxima profiles were essentially identical to those of MBTD treated with NO (Figure 1A,B). Besides, HPLC-MS analysis showed that treating MBTD with NO quantitatively produced a new product with the same mass peak and retention time as those of MBTT (Figures S7B and S8A). Obviously, these results suggested that reaction of MBTD with NO in pH 5.0 PB buffer produced the benzotriazole product MBTT, which was in good agreement with the mechanism proposed in Scheme 1.

NO-dependent changes of the MBTD absorption and emission spectra were further investigated by adjusting the concentration of NO. Along with the increase of NO concentration up to 100 μM, the intensity of the 488 nm absorbance (ε = 11600 M^{-1} cm^{-1}) increased gradually while the 365 nm absorption decreased with an obvious isoabsorption point at 421 nm (Figure 1C). Meanwhile, two characteristic fluorescence bands appeared at 550 and 625 nm in the emission spectra (λ_{ex} = 421 nm). Interestingly, the 625 nm emission enhanced gradually while the 550 nm emission kept constant (Figure 1D), indicating a ratiometric fluorescence response of MBTD probe. The maximal UV−vis absorbance at 488 nm and its emission at 625 nm linearly increased in a concentration-dependent manner in a wide NO concentration range, with detection limits of 1.2 and 1.1 μM (3σ/slope), respectively (Figure S9B−D). In particularly, the 625 to 550 nm fluorescence ratios (F_{625nm}/F_{550nm}) increased linearly as a function of NO concentration with an improved detection limit of 0.71 μM (Figure 1D). To keep consistence with that of imaging application, the F_{625nm}/F_{565nm} ratio upon excitation at 488 and 405 nm, respectively, were also shown (Figure S10). These results suggested the potential of MBTD for NO detection by both colorimetry and fluorescence ratiometry in far-red emission region.

To examine the NO specificity of MBTD, we inspected the F_{625nm}/F_{550nm} ratios of MBTD with the addition of a wide array of the potentially interfering substances, which were categorized as reactive oxygen/nitrogen species (ROS/RNS: NO_2^-, NO_3^-, $^{\bullet}OH$, ClO^-, TBHP, H_2O_2, $O_2^{\bullet-}$, $^1O_2$ and $ONOO^-$), metal ions (K^+, Na^+, Ca^{2+}, Mg^{2+}, Fe^{2+}, Fe^{3+}, and Zn^{2+}), and active biomolecules (GSH, Cys, Hcy, ascorbic acid (AA) and dehydroascorbic acid (DHA)). All the interfering substances showed negligible influence on MBTD fluorescence, while only NO remarkably increased the F_{625nm}/F_{550nm} fluorescence ratio (Figure 2A), suggesting high NO selectivity of MBTD, which could be most likely explained by the relative low reactivity of electron-withdrawing TOPD functionality.

The real-time fluorescence intensity variations of MBTD probe toward NO was tested by recording the fluorescent intensity at two emission wavelengths of 550 and 625 nm, respectively. Upon addition of 100 μM NO, the fluorescence intensity at 550 nm was weak, and kept intact during 180 min (Figure S11A). In contrast, the emission intensity at 625 nm remarkably increased and quickly reached a plateau within 20 min, with a 33-fold enhancement in comparison with the basal level. The fluorescence signal kept steady for several hours (>2 h), verifying the potential of MBTD for real-time fluorescence imaging of biological NO (Figure 2B). The fluorescence lifetime measurement revealed that the average lifetime of MBTD determined by multiexponential fitting was 2.68 ns, while MBTT displayed a longer lifetime up to 7.91 ns, which could avoid the interference of background fluorescence and photobleaching (Figure S11B). These results showed that MBTT possessed a persistent fluorescent emission for a long-term fluorescence imaging.

In the assessment of pH responses of MBTD toward NO, it was found that the F_{625nm}/F_{550nm} fluorescence ratios of MBTD were nearly 1.0 with negligible variation throughout the tested pH range of 4.5−9.0 (Figure 2C), indicating its high tolerance

DOI: 10.1021/acs.analchem.8b00612
Anal. Chem. XXXX, XXX, XXX−XXX

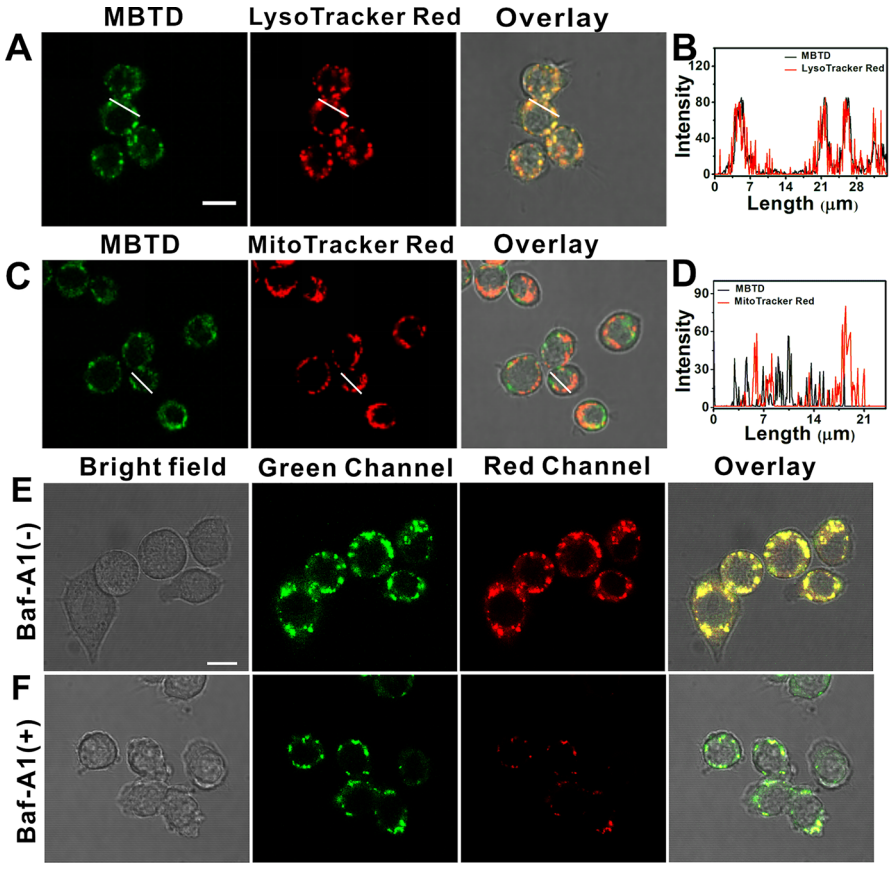

Figure 3. (A, C) Colocalization of MBTD with the lysosomal (A) and (C) mitochondrial vesicles in RAW 264.7 cells. (B, D) The corresponding intensity profiles. (A–D, probe channel: λ_{ex} = 405 nm λ_{em} = 520–570 nm. Red channel: λ_{ex} = 552 nm; λ_{em} = 590–700 nm). (E) MBTD-loaded cells incubated with 200 μM DEANO for 1 h. (F) 1 μM Baf-A1-pretreated cells treated with 5 μM MBTD followed by incubation with 200 μM DEANO. (E, F) Green channel: λ_{ex} = 405 nm, λ_{em} = 520–570 nm. Red channel: λ_{ex} = 488 nm, λ_{em} = 590–650 nm. Scale bar = 10 μm.

in a wide pH range with low background fluorescence. In the presence of excessive NO (2 equiv), the F_{625nm}/F_{550nm} ratios were significantly enhanced under acidic conditions in a pH-dependent manner, and reached to the maxima in the pH range of 4.5–5.0, which is in good accordance with the lysosomal acidity (e.g., pH < 6.0), while it dropped to a comparable baseline-level to that of free MBTD under alkaline conditions (pH > 8.0). HPLC-MS analytic results showed that MBTD react with NO in pH 5.0 buffer solution to generate MBTT (Figures S8A and S7), while the reaction failed in pH 9.0 buffer solution, and most of MBTD still remained (Figures S8B and S12). Given the fact that MOBTD without the morpholinyl group also displayed a similar pH-dependent NO response (Figure S11D), this unique pH-dependent reactivity of MBTD with NO is probably attributed to the blunt nucleophilic ability of TOPD, which reacts only with NO in acidic conditions, but not with alkaline NO. These results revealed that MBTD is an acid-promoted and acid-tolerant fluorescent probe for intracellular NO determination in the acidic lysosome. Besides, the triazole product MBTT also displayed a similar pH-dependent fluorescence emission curve with the calculated pK_a value of 5.6 (Figure S11C). The remarkable reduction in the fluorescence intensity under nonacidic condition was probably ascribed to the formation of the triazolate MBTT-H$^+$ as a weak electron acceptor (Scheme 3).

To validate the reaction mechanism we proposed in Scheme 1, the highest occupied molecular orbitals (HOMO), lowest unoccupied molecular orbitals (LUMO), and band gap levels of MBTD and MBTT were obtained from density functional theory (DFT) calculations in the gas phase. As shown in Table 1, the HOMOs of these two compounds were essentially delocalized on the whole molecular backbone, and the LOMOs were mainly distributed on the electron accepting unit (thiadiazole-fused benzotriazole). Moreover, MBTT presented higher-lying calculated HOMO and LUMO levels, and displayed lower bandgap than MBTD, which may account for the relatively stronger ICT effect that led to the large red-shift of the exciting/emission wavelengths. It was also found that the HOMO–LUMO bandgap of MBTT-H$^+$ was larger than that of MBTT, indicating the attenuation of ICT process induced by the deprotonation of the triazole in the electron accepting unit.

Fluorescence Imaging of NO in Living Cells. Both MBTD and MBTT showed negligible cytotoxicity in RAW 264.7 cells at the concentrations from 1 to 15 μM as revealed by MTT assay (Figure S13). We began to investigate the imaging ability of the probe at different times by CLSM examination (Figure S14). After 40 min, a strong red fluorescence was observed. We next evaluated the lysosome-targeting ability of the MBTD probe. The intracellular lysosomal vesicles and mitochondria of RAW 264.7 cells were stained with LysoTracker Red or MitoTracker Red, respectively. Figure 3A–D showed that in the absence of exogenous NO, the cells displayed noticeable green fluorescence post 1 h incubation with MBTD at 37 °C. The green fluorescence emission of MBTD colocalized well with the red fluorescence signal of LysoTracker Red while not MitoTracker Red. The

DOI: 10.1021/acs.analchem.8b00612
Anal. Chem. XXXX, XXX, XXX–XXX

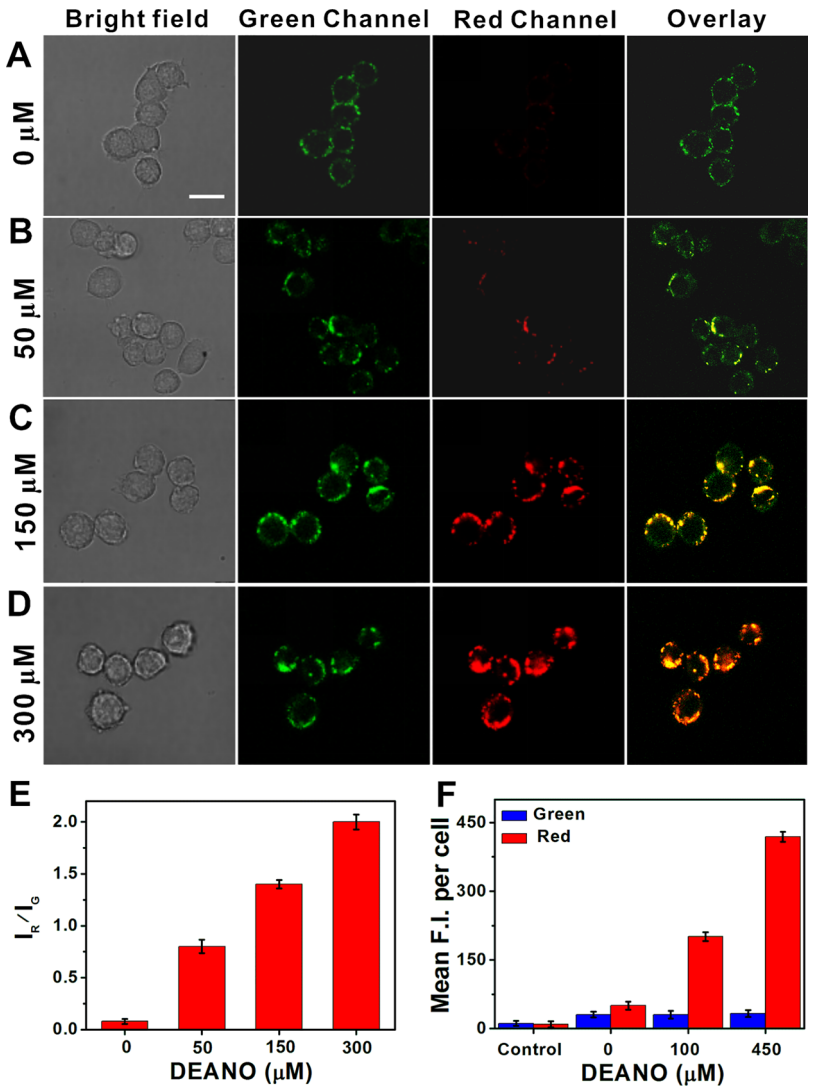

Figure 4. (A–D) CLSM imaging of RAW 264.7 cells treated with MBTD at various DEANO concentration (0, 50, 150, 300 μM) for 1 h. (E) The ratiometric intensity of red/green fluorescence as a function of DEANO concentration. Green channel: λ_{ex} = 405 nm, λ_{em} = 520–570 nm. Red channel: λ_{ex} = 488 nm, λ_{em} = 590–650 nm. (F) Flow cytometric analysis results. λ_{ex} = 355 nm, λ_{em} = 515–545 nm; Red channel: λ_{ex} = 488 nm, λ_{em} = 564–606 nm. Scale bar = 10 μm.

intensity profiles of the linear regions of interest across the cells that stained with MBTD and LysoTracker Red varied in very close synchrony with Pearson's colocalization coefficient and overlap coefficient of 0.83 and 0.99, respectively, while those stained with MBTD and MitoTracker Red varied in remarkable inconsistency (Figure 3B,D). In contrast, MOBTD without the morpholinyl group poorly colocalized with the lysosomal vesicles, indicating poor lysosome specificity (Figure S15), and the morpholinyl group accounts for the excellent lysosome-targeting ability of MBTD.

To investigate the ability of MBTD to image NO in the lysosomes, the MBTD-loaded cells were incubated with DEANO, an exogenous NO donor, for 1 h. As shown in Figure 3E, remarkable green and red fluorescence were observed in the lysosome, respectively. Upon pretreatment with NO scavenger hemoglobin (Hb), the cells showed barely detectable red fluorescence, verifying the increased fluorescence emission could be attributed to the presence of lysosomal NO (Figure S16). To further demonstrate if it could specifically response to the coexistence of H^+ and NO in the lysosome, RAW 264.7 cells were pretreated with Baf-A1, a H^+-ATPase inhibitor to neutralize the acidic surrounding of the lysosome. As expected, no obvious red fluorescence was observed and only weak green fluorescence remained after incubation with MBTD in the presence of NO (Figure 3F), indicating that the intracellular response behavior of the MBTD probe toward NO happened specifically in the acidic lysosomes rather than in other nonacidic organelles. The ability of MBTD to monitor the dynamic pH changes of lysosome in RAW 264.7 cells in the presence of DEANO was investigated (Figure S17). It was found that red fluorescence gradually decreased with the increase of the lysosomal pH value, indicating the potential of MBTD for monitoring lysosomal pH changes.

CLSM examination was further performed to investigate the feasibility of MBTD for the ratiometric measurement of the lysosomal NO. In absence of NO, the probe-loaded cells showed noticeable green fluorescence without the appearance of red fluorescence (Figure 4A). Intracellular red fluorescence was observed post 1 h incubation of the cells with 50 μM DEANO as exogenous NO donor (Figure 4B). Moreover, the red fluorescence increased gradually with the increase of DEANO concentrations (Figure 4C,D). The relative fluores-

DOI: 10.1021/acs.analchem.8b00612
Anal. Chem. XXXX, XXX, XXX–XXX

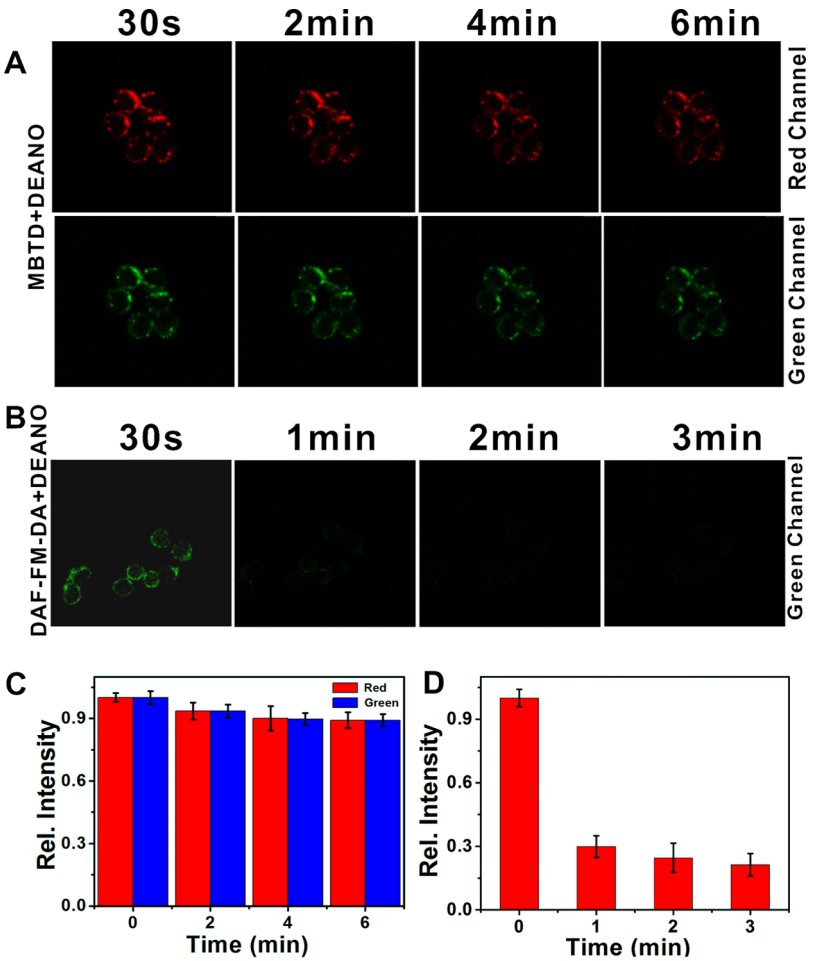

Figure 5. (A) MBTD and (B) DAF-FM-DA-mediated dynamic CLSM examination of exogenous NO in RAW 264.7 cells (Green channel: λ_{ex} = 405 nm, λ_{em} = 520−570 nm; Red channel: λ_{em} = 488 nm, λ_{em} = 590−650 nm; Scale bar = 10 μm). (C, D) Relative fluorescence intensities of MBTD (C) and DAF-FM-DA (D) along with time, respectively.

cent intensity ratio (I_R/I_G) displayed a positive correlation with DEANO concentration ranging from 0 to 300 μM (Figure 4E).

Flow cytometric measurement was performed to demonstrate the potential of MBTD probe for quantitative detection of exogenous NO. Compared to the control cells without staining, cells incubated with MBTD alone show marginally detectable fluorescence intensity. The red fluorescence increased upon DEANO incubation at 100 or 450 μM, without affecting the intensity of green fluorescence (Figures 4F and S18). Accordingly, the CLSM and flow cytometric data consistently suggested the good potential of MBTD for accurately monitoring the variation of exogenous NO. As shown in Figures S19 and S20, MCF-7 and HepG2 cells were also used to image NO in living cells. The results confirm the imaging capability of MBTD probe in other cells lines.

The photostability of MBTD after incubation with DEANO in RAW 264.7 cells was assessed under laser irradiation at 405 and 488 nm, respectively. A commercially available NO probe DAF-FM-DA was selected as a parallel control.[55] Figure 5A,C showed negligible fluctuation in both red and green fluorescence intensity upon laser irradiation for 6 min. In contrast, when the cells were treated with DAF-FM-DA and DEANO, the green fluorescence decayed gradually at 30 s, and completely disappeared within 3 min (Figure 5B,D). These results indicate that MBTD possesses much better fluorescence stability than DAF-FM-DA probe, allowing for continuously monitoring the dynamic change of NO in living cells for a long period.

We next sought to testify the feasibility of MBTD for measuring endogenous NO in vitro. Cells were stimulated with lipopolysaccharide (LPS) and then treated with MBTD. Figure S21A showed LPS stimulation followed by MBTD incubation led to a marked enhancement in red fluorescence (Figure S21B). To verify whether the enhanced fluorescence could be attributed to LPS-induced massive endogenous NO, the cells were coincubated with LPS and Hb, and subsequently treated with MBTD probe. The CLSM image exhibited a barely detectable red fluorescence (Figure S21C), as indicated by 2.5-D image and I_R/I_G ratio histogram, respectively (Figure S21D,E). These results clarify the potential of MBTD probe for ratiometric detection of the endogenous NO in living cells.

Ex Vivo Imaging of NO in an Acute Liver Injury Mouse Model. After confirming the ability of MBTD to track both exogenous and endogenous NO in living cells, we further explored its potential for in situ detection of the lysosomal NO in an acute liver injury mouse model (Figure 6A). The Balb/c mice were intraperitoneally (i.p.) injected with LPS and D-galactosamine (D-GalN) at a dose of 5 μg/kg and 300 mg/kg, respectively. The mice were sacrificed at 4 h post-injection. Haematoxylin-eosin (H&E) staining of the liver sections showed significant vacuolization of the hepatic parenchymal cells, verifying LPS-induced inflammation of the liver tissue

DOI: 10.1021/acs.analchem.8b00612
Anal. Chem. XXXX, XXX, XXX−XXX

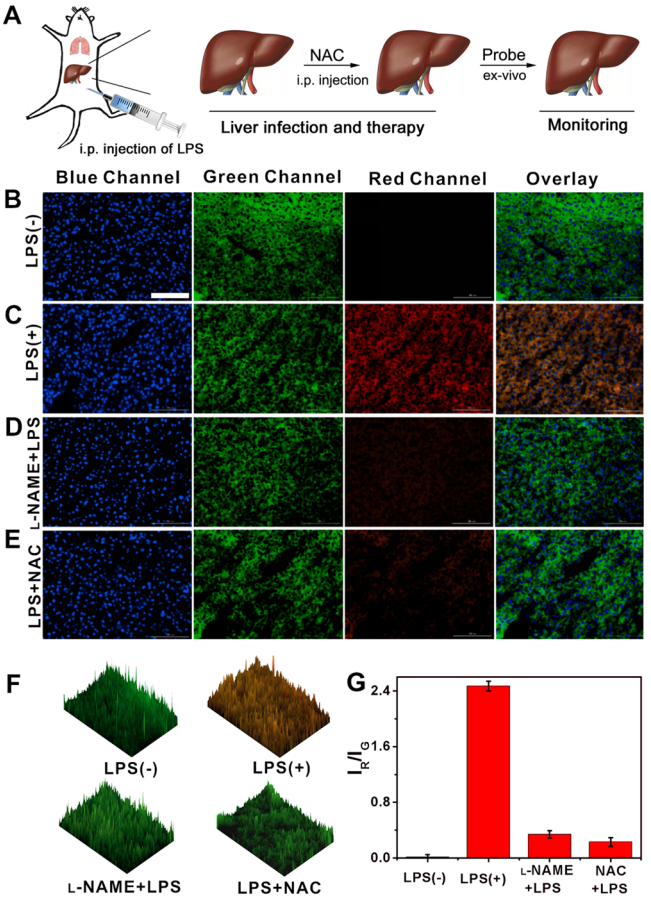

Figure 6. (A) Experimental schedule for MBTD-mediated fluorescence examination of endogenous NO in an inflamed mouse model. (B) The saline group. (C) LPS/D-GalN-induced inflammed mice group. (D) L-NAME-treated infection mice group. (E) NAC-treated infection mice group. Scale bar = 100 μm in B–E. (F) 2.5D images of B, C, D, and E groups, respectively. (G) The I_R/I_G fluorescence intensity ratio of B–E groups. Blue channel: λ_{ex} = 377 nm, λ_{em} = 410–480 nm; Green channel: λ_{ex} = 469 nm, λ_{em} = 495–570 nm; Red channel: λ_{ex} = 531 nm, λ_{em} = 550–650 nm.

(Figure S22). As vividly illustrated in Figure 6B, the MBTD-stained liver slices of unstimulated mice displayed measurable green fluorescence in the saline-injected control group, and negligible red fluorescence was observed in red channel. The image of the liver slice of the inflamed mice exhibited a notably enhanced red fluorescence with an I_R/I_G value of 2.4 (Figure 6C), indicating the generation of the massive endogenous NO.

It was reported that the overactivation of iNOS during the infection and inflammation was mainly responsible for the production of NO and other reactive nitrogen species.[56,57] To determine if the aforementioned red fluorescence enhancement was induced by in vivo generated NO, the mice were pretreated with an iNOS inhibitor N-nitro-arginine methyl ester (L-NAME) for 6 h, and then with 5 μg/kg LPS and 300 mg/kg D-GalN. CLSM examination in Figure 6D showed a dramatic decrease of red fluorescence with an I_R/I_G ratio of 0.3 due to the suppressed NO generation by L-NAME, further suggesting the great potential of MBTD to investigate the regulation mechanism of endogenous NO by iNOS in the inflammation.

NO has been defined as one of indicators reflecting the degree of inflammation.[58,59] Meanwhile, N-acetylcysteine (NAC) is a FDA-approved drug for clinical treatment of the drug-induced acute liver injury. We thus attempted to explore the potential application of MBTD probe for real-time monitoring the therapeutic efficacy of NAC. As shown in Figure 6E, treatment of the liver injured mice with NAC led to a markedly decreased red fluorescence with a lower I_R/I_G value of 0.2, illustrating that NAC could effectively alleviate the liver injury of the inflamed mice leading to a significantly decreased NO level. Both the 2.5D CLSM images and I_R/I_G ratio histogram vividly displayed the variation of the relative fluorescence intensity related with the NO levels in the inflammed mice with different treatment (Figure 6F,G). The above results demonstrate the promising potential of MBTD probe for in situ monitoring the therapeutic efficacy by detecting the variation of pathological NO.

CONCLUSIONS

In summary, we have developed a novel fluorescent NO probe MBTD with far-red emission based on a dual ICT mechanism by merging of the OPD moiety into the D-A-D type fluorophore. MBTD possesses several distinct merits including large fluorescence on–off ratio, long-lived fluorescence with better stability, and high specificity for NO over other disturbing species. Moreover, MBTD is featured by lysosomal acid-compatible properties for specific imaging of lysosomal NO. All these distinct advantages collectively enable it to accurately detect the variation of both exogenous and endogenous NO levels in cells. More importantly, the probe is able to monitor the variation of lysosomal NO level in the inflamed mouse model, which not only reveals iNOS is critically responsible for NO generation in the inflamed liver, but also suggests that NO is one of important therapeutic indicators of acute liver injury. Taken together, MBTD as a novel type of NO probe might open a new avenue for precisely detecting lysosomal NO-related biological process.

ASSOCIATED CONTENT

Supporting Information

The Supporting Information is available free of charge on the ACS Publications website at DOI: 10.1021/acs.analchem.8b00612.

Synthesis, flow cytometric examination, theoretical calculation, and supplementary figures (PDF).

AUTHOR INFORMATION

Corresponding Authors

*E-mail: zaxu@chem.ecnu.edu.cn. Tel./Fax: +86-21-54340053.
*E-mail: chding@simm.ac.cn. Tel./Fax: +86-21-50806600.

ORCID

Zhiai Xu: 0000-0002-4391-2507
Yi Luo: 0000-0001-6390-8639
Zhen Cheng: 0000-0001-8177-9463
Haijun Yu: 0000-0002-3398-0880
Ao Zhang: 0000-0001-7205-9202
Chunyong Ding: 0000-0003-2379-8740

Author Contributions

†These authors contributed equally to this work (F.W. and S.Y.).

Notes

The authors declare no competing financial interest.

DOI: 10.1021/acs.analchem.8b00612
Anal. Chem. XXXX, XXX, XXX–XXX

■ ACKNOWLEDGMENTS

The authors thank the assistance from Prof. Guang Liang at Wenzhou Medical University for in vivo liver infection model, and Dr. Chengyuan Peng and Prof. Ruimin Huang at SIMM for cell imaging. Financial supports by the National Natural Science Foundation of China (Nos. 21675055, 81402790, 21775046, 21635003) are greatly appreciated. Financial supports from the International Cooperative Program of the Chinese Academy of Sciences (GJHZ1622) and the Key Program of the Frontier Science of the Chinese Academy of Sciences (160621) were also appreciated.

■ REFERENCES

(1) Fukumura, D.; Kashiwagi, S.; Jain, R. K. *Nat. Rev. Cancer* **2006**, *6*, 521−534.
(2) Calabrese, V.; Mancuso, C.; Calvani, M.; Rizzarelli, E.; Butterfield, D. A.; Stella, A. M. G. *Nat. Rev. Neurosci.* **2007**, *8*, 766−775.
(3) Mel, A.; Murad, F.; Seifalian, A. M. *Chem. Rev.* **2011**, *111*, 5742−5767.
(4) Szabo, C. *Nat. Rev. Drug Discovery* **2016**, *15*, 185−203.
(5) Bashan, N.; Kovsan, J.; Kachko, I.; Ovadia, H.; Rudich, A. *Physiol. Rev.* **2009**, *89*, 27−71.
(6) Rabinowitz, J. D.; White, E. *Science* **2010**, *330*, 1344−1348.
(7) Pluth, M. D.; Tomat, E.; Lippard, S. J. *Annu. Rev. Biochem.* **2011**, *80*, 333−355.
(8) Shintani, T.; Klionsky, D. J. *Science* **2004**, *306*, 990−995.
(9) Levine, B.; Klionsky, D. J. *Dev. Cell* **2004**, *6*, 463−477.
(10) Pacher, P.; Beckman, J. S.; Liaudet, L. *Physiol. Rev.* **2007**, *87*, 315−424.
(11) Sarkar, S.; Korolchuk, V. I.; Renna, M.; Imarisio, S.; Fleming, A.; Williams, A.; Garcia-Arencibia, M.; Rose, C.; Luo, S.; Underwood; Benjamin, R.; Kroemer, G.; O'Kane, C. J.; Rubinsztein; David, C. *Mol. Cell* **2011**, *43*, 19−32.
(12) Han, F.; Chen, Y. X.; Lu, Y. M.; Huang, J. Y.; Zhang, G. S.; Tao, R. R.; Qin, Z. H. *J. Pineal Res.* **2011**, *51*, 124−135.
(13) Yu, H.; Xiao, Y.; Jin, L. *J. Am. Chem. Soc.* **2012**, *134*, 17486−17489.
(14) Zhang, H. X.; Chen, J. B.; Guo, X. F.; Wang, H.; Zhang, H. S. *Anal. Chem.* **2014**, *86*, 3115−3123.
(15) Adarsh, N.; Krishnan, M. S.; Ramaiah, D. *Anal. Chem.* **2014**, *86*, 9335−9342.
(16) Chen, Z.; Li, Q.; Sun, Q.; Chen, H.; Wang, X.; Li, N.; Tang, B. *Anal. Chem.* **2012**, *84*, 4687−4694.
(17) Sun, J.; Yan, Y.; Sun, M.; Yu, H.; Zhang, K.; Huang, D.; Wang, S. *Anal. Chem.* **2014**, *86*, 5628−5632.
(18) Kojima, H.; Urano, Y.; Kikuchi, K.; Higuchi, T.; Hirata, Y.; Nagano, T. *Angew. Chem., Int. Ed.* **1999**, *38*, 3209−3212.
(19) Tan, L.; Wan, A.; Li, H. *Langmuir* **2013**, *29*, 15032−15042.
(20) Xu, Q.; Liu, W.; Li, L.; Zhou, F.; Zhou, J.; Tian, Y. *Chem. Commun.* **2017**, *53*, 1880−1883.
(21) Chen, X.; Pradhan, T.; Wang, F.; Kim, J. S.; Yoon, J. *Chem. Rev.* **2012**, *112*, 1910−1956.
(22) Yu, H.; Xiao, Y.; Jin, L. *J. Am. Chem. Soc.* **2012**, *134*, 17486−17489.
(23) Sun, Y. Q.; Liu, J.; Zhang, H.; Huo, Y.; Lv, X.; Shi, Y.; Guo, W. *J. Am. Chem. Soc.* **2014**, *136*, 12520−12523.
(24) Dong, X.; Heo, C. H.; Chen, S.; Kim, H. M.; Liu, Z. *Anal. Chem.* **2014**, *86*, 308−311.
(25) Yuan, L.; Lin, W.; Xie, Y.; Chen, B.; Zhu, S. *J. Am. Chem. Soc.* **2012**, *134*, 1305−1315.
(26) Wang, C.; Song, X.; Han, Z.; Li, X.; Xu, Y.; Xiao, Y. *ACS Chem. Biol.* **2016**, *11*, 2033−2040.
(27) Yuan, L.; Lin, W.; Xie, Y.; Chen, B.; Song, J. *Chem. Commun.* **2011**, *47*, 9372−9374.
(28) Wu, P.; Wang, J.; He, C.; Zhang, X.; Wang, Y.; Liu, T.; Duan, C. *Adv. Funct. Mater.* **2012**, *22*, 1698−1703.
(29) Sun, X.; Xu, Y.; Zhu, W.; He, C.; Xu, L.; Yang, Y.; Qian, X. *Anal. Methods* **2012**, *4*, 919−922.
(30) Vegesna, G. K.; Sripathi, S. R.; Zhang, J.; Zhu, S.; He, W.; Luo, F.-T.; Jahng, W. J.; Frost, M.; Liu, H. *ACS Appl. Mater. Interfaces* **2013**, *5*, 4107−4112.
(31) Yao, H.-W.; Zhu, X.-Y.; Guo, X.-F.; Wang, H. *Anal. Chem.* **2016**, *88*, 9014−9021.
(32) Adarsh, N.; Krishnan, M. S.; Ramaiah, D. *Anal. Chem.* **2014**, *86*, 9335−9342.
(33) Cao, Y.; Li, D. W.; Zhao, L. J.; Liu, X. Y.; Cao, X. M.; Long, Y. T. *Anal. Chem.* **2015**, *87*, 9696−9701.
(34) Li, D. W.; Qu, L. L.; Hu, K.; Long, Y. T.; Tian, H. *Angew. Chem., Int. Ed.* **2015**, *54*, 12758−12761.
(35) Cui, J.; Hu, K.; Sun, J. J.; Qu, L. L.; Li, D. W. *Biosens. Bioelectron.* **2016**, *85*, 324−330.
(36) Nagano, T.; Yoshimura, T. *Chem. Rev.* **2002**, *102*, 1235−1270.
(37) Reja, S. I.; Gupta, M.; Gupta, N.; Bhalla, V.; Ohri, P.; Kaur, G.; Kumar, M. *Chem. Commun.* **2017**, *53*, 3701−3704.
(38) Li, Y.; Wu, W.; Yang, J.; Yuan, L.; Liu, C.; Zheng, J.; Yang, R. *Chem. Sci.* **2016**, *7*, 1920−1925.
(39) Chen, X.; Wang, F.; Hyun, J. Y.; Wei, T.; Qiang, J.; Ren, X.; Yoon. *Chem. Soc. Rev.* **2016**, *45*, 2976−3016.
(40) Xu, Q.; Liu, W.; Li, L.; Zhou, F.; Zhou, J.; Tian, Y. *Chem. Commun.* **2017**, *53*, 1880−1883.
(41) Dai, Z.; Tian, L.; Song, B.; Liu, X.; Yuan, J. *Chem. Sci.* **2017**, *8*, 1969−1976.
(42) Li, H.; Zhang, D.; Gao, M.; Huang, L.; Tang, L.; Li, Z.; Chen, X.; Zhang, X. *Chem. Sci.* **2017**, *8*, 2199−2203.
(43) Mao, Z.; Jiang, H.; Li, Z.; Zhong, C.; Zhang, W.; Liu, Z. *Chem. Sci.* **2017**, *8*, 4533−4538.
(44) Mao, Z.; Feng, W.; Li, Z.; Zeng, L.; Lv, W.; Liu, Z. *Chem. Sci.* **2016**, *7*, 5230−5235.
(45) Wang, B.; Yu, S.; Chai, X.; Li, T.; Wu, Q.; Wang, T. *Chem. - Eur. J.* **2016**, *22*, 5649−5656.
(46) Huo, Y.; Miao, J.; Han, L.; Li, Y.; Li, Z.; Shi, Y.; Guo, W. *Chem. Sci.* **2017**, *8*, 6857−6864.
(47) Wang, N.; Yu, X.; Zhang, K.; Mirkin, J. *J. Am. Chem. Soc.* **2017**, *139*, 12354−12357.
(48) Ono, K.; Tanaka, S.; Yamashita, Y. *Angew. Chem., Int. Ed. Engl.* **1994**, *33*, 1977−1979.
(49) Patel, D. G.; Feng, F.; Ohnishi, Y.; Abboud, K. A.; Hirata, S.; Schanze, K. S.; Reynolds, J. R. *J. Am. Chem. Soc.* **2012**, *134*, 2599−2612.
(50) Qian, G.; Zhong, Z.; Luo, M.; Yu, D.; Zhang, Z.; Ma, D.; Wang, Z. Y. *J. Phys. Chem. C* **2009**, *113*, 1589−1595.
(51) Antaris, A. L.; Chen, H.; Cheng, K.; Sun, Y.; Hong, G.; Qu, C.; Diao, S.; Deng, Z.; Hu, X.; Zhang, B.; Zhang, X.; Yaghi, O.; Alamparambil, Z. R.; Hong, X.; Cheng, Z.; Dai, H. *Nat. Mater.* **2016**, *15*, 235−242.
(52) Zhu, S.; Yang, Q.; Antaris, A. L.; Yue, J.; Ma, Z.; Wang, H.; Huang, W.; Wan, H.; Wang, J.; Diao, S.; Zhang, B.; Li, X.; Zhong, Y.; Yu, K.; Hong, G.; Luo, J.; Liang, Y.; Dai, H. *Proc. Natl. Acad. Sci. U. S. A.* **2017**, *114*, 962−967.
(53) Antaris, A. L.; Chen, H.; Diao, S.; Ma, Z.; Zhang, Z.; Zhu, S.; Wang, J.; Lozano, A. X.; Fan, Q.; Chew, L.; Zhu, M.; Cheng, K.; Hong, X.; Dai, H.; Cheng, Z. *Nat. Commun.* **2017**, *8*, 15269.
(54) Sun, Y.; Ding, M.; Zeng, X.; Xiao, Y.; Wu, H.; Zhou, H.; Zhang, Y.; Chen, Z.; Hong, X. *Chem. Sci.* **2017**, *8*, 3489−3493.
(55) Wei, P.; Ma, P.; Xu, Q. S.; Bai, Q. H.; Gu, J. G.; Xi, H.; Yu, C. *Glycoconjugate J.* **2012**, *29*, 285−295.
(56) Moncada, S.; Bolaños, J. P. *J. Neurochem.* **2006**, *97*, 1676−1689.
(57) Iwakiri, Y.; Satoh, A.; Chatterjee, S.; Toomre, D. K.; Chalouni, C. M.; Fulton, D.; Roberto, J. G.; Vijay, H. S.; Sessa, W. C. *Proc. Natl. Acad. Sci. U. S. A.* **2006**, *103*, 19777−19782.
(58) Butler, A. R.; Williams, D. L. H. *Chem. Soc. Rev.* **1993**, *22*, 233−241.
(59) Bogdan, C. *Nat. Immunol.* **2001**, *2*, 907−916.

DOI: 10.1021/acs.analchem.8b00612
Anal. Chem. XXXX, XXX, XXX−XXX